The Destruction of Lenses and Generation of Wodons

CHUAN SHI*

Department of Oceanography, The Florida State University, Tallahassee, Florida

DORON NOF

Department of Oceanography and the Geophysical Fluid Dynamics Institute, The Florida State University, Tallahassee, Florida

(Manuscript received 5 March 1993, in final form 21 June 1993)

ABSTRACT

Since midocean eddies migrate westward, they eventually reach the western boundaries. It is, therefore, of interest to find out what happens after the eddies collide with the walls. An isopycnic, two-layer, primitive equation model on a β plane and a simple analytical model on an f plane are constructed to investigate the meridional migration of an oceanic eddy along a western wall.

On a β plane, three factors determine the eddy's migration along a western meridional wall. First, the image effect pushes an anticyclonic (cyclonic) eddy northward (southward). Second, the β force (resulting from the larger Coriolis force on the northern side of the eddy) pulls an anticyclonic (cyclonic) eddy southward (northward). Third, after an anticyclonic (cyclonic) eddy collides with the wall, parts of the anticyclonic eddy's interior fluid leak out southward (northward) along the wall forming a thin jet. In an analogy to a rocket, this jet pushes the eddy northward (southward). Our aim is to investigate in which direction the eddy ultimately migrates along the wall (i.e., to determine which of the above three processes dominates).

The combined effect of the three processes is a rather complicated process and the results are counterintuitive. For instance, imagine a lenslike anticyclonic eddy situated on a sloping bottom (analogous to β). This highly nonlinear eddy migrates with shallow water on its right ("westward") and encounters a meridional wall. Intuitively, it is expected that, once the "westward" migration is arrested by the wall, gravity will pull the eddy downhill (southward) so that the eddy will migrate toward deep water (i.e., toward the equator). Surprisingly, however, the authors' numerical computations show that the eddy migrates *uphill*. This bizarre behavior results from the leakage along the wall that, in terms of the eddy energy, compensates for the uphill drift. Namely, the leakage plays a crucial role in the eddy–wall interaction process because it allows the uphill migration. Eventually, it causes a destruction of the lens by completely draining its fluid.

The above highly nonlinear experiments are supplemented by quasigeostrophic analytical solutions and isopycnic numerical experiments of cyclones and anticyclones. It is found that, in contrast to the situation with the lens, the leakage does not play a crucial role in quasigeostrophic eddies. However, all of these experiments show that the image effect is the most dominant process. It turns out that, as the eddy responds to the presence of the wall, it is transformed into a half-circular shape that is very different from its original preinteraction circular shape. This results from the fact that, even though the westward β-induced speed (forcing the eddy into the wall) is small, it is active over an extended period of time so that its final effect is relatively large. The final half-circular eddy that migrates along the wall is nearly independent of β as long as the eddy is not extremely far from its original latitude. This is demonstrated by both our numerical solution (of the primitive equations) as well as our quasigeostrophic analytical solution. The authors term this final migrating eddy a *wodon* as it represents a combination of a *w*all and a m*odon*.

Possible applications of these models to various oceanic situations are discussed.

1. Introduction

In an open ocean, mesoscale eddies continuously migrate westward due to β. It is therefore of interest to investigate an eddy's migration after it encounters a western continental slope. Recent observations obtained from satellite or buoy drifters show a complex migration pattern for eddies adjacent to the continental slopes. For example, Fig. 1 [adapted from Evans et al. (1985)] illustrates the location of the center track for Gulf Stream warm core ring 82B. This anticyclonic ring first moved westward, and then southwestward (along the isobaths) at an average speed of 3 km day^{-1}. Figure 2 [adapted from Kirwan et al. (1988)], on the other hand, demonstrates that the center motion of an anticyclonic Loop Current ring in the western Gulf of Mexico first migrated westward, and then translated

* Current affiliation: Horn Point Environmental Laboratory, University of Maryland, Cambridge, Maryland.

Corresponding author address: Dr. Chuan Shi, Horn Point Environmental Laboratory, University of Maryland, Cambridge, MD 21613.

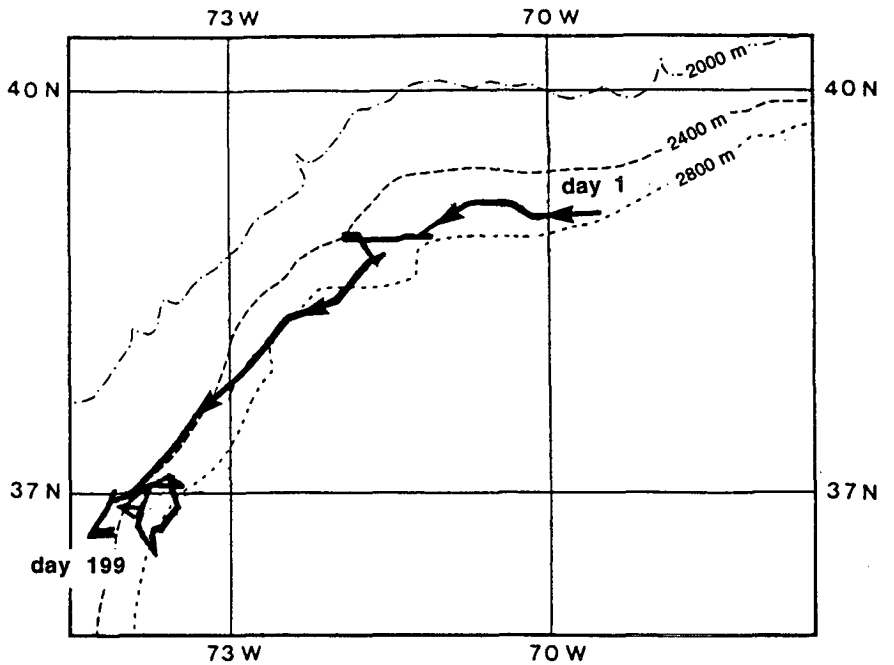

FIG. 1. The drift of a Gulf Stream warm core ring 82B near the western Atlantic continental slope (adapted from Evans et al. 1985). It illustrates that the eddy first moves westward and then southwestward along the continental slope.

northward at a speed of 3.5 km day^{-1}. Ultimately, the ring slowly turned away from the slope, and changed its migration direction from northward to southward. From these two very different observations, it is clear that an eddy's migration near western boundaries is a very complex process. The question that we will address

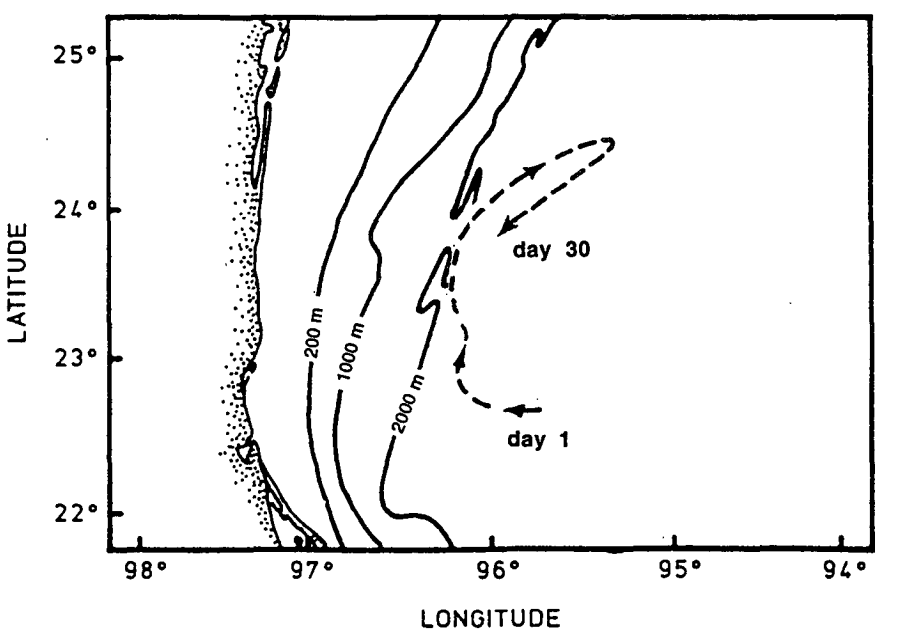

FIG. 2. The center motion of a Loop Current anticyclonic ring near the continental slope of the western Gulf of Mexico (adapted from Kirwan et al. 1988). It shows that, initially, the eddy migrated westward. It then turned 90° to the north and northeast along the slope and then turned again and moved southwestward.

in this study is what mechanisms determine the final eddy migration along a western boundary.

To understand the complicated near-wall migration process, it is assumed that a western continental slope can be approximated by a meridional vertical wall. For simplicity, we shall first examine an anticyclonic (or cyclonic) eddy next to a wall above an infinitely deep upper layer (Fig. 3). In a 1½-layer model, three factors determine an eddy's meridional migration next to a wall. First, the so-called image effect (i.e., the eddy's advection along a free-slip wall due to its image) pushes the anticyclone (cyclone) northward (southward). Second, since the Coriolis force acting on particles in the northern part of the eddy is larger than that in the southern part of the anticyclonic (cyclonic) eddy, a southward (northward) net force is established (hereafter, this force is referred to as the β force). Third, as the β-induced *western* drift (to be distinguished from the meridional drift due to β) continues to force the eddy toward the wall, part of the anticyclonic (cyclonic) eddy's fluid flows southward (northward) along the wall forming a thin jet (Fig. 3, see also Nof 1988a,b). In an analogy to a rocket, this thin jet gives the eddy a northward (southward) momentum. In short, the image effect and the "rocket" effect try to push an anticyclone northward, while the β force tends to pull it southward. Similarly, a cyclone is pulled southward by the image effect and the "rocket" effect, but is pushed northward by the β force.

A general scaling analysis suggests that all three migration mechanisms induce speeds of roughly the same order. Hence, it is impossible to tell in advance at which direction an eddy will eventually propagate as a reaction to the presence of a wall. It turns out, however, that, at least in all the cases that we have looked at, the image effect always dominates.

The complexity of the eddy migration along the wall is apparent not only from the scaling mentioned above. From a theoretical point of view it is perhaps best illustrated by the reaction of a lens to the presence of a wall. Consider the situation shown in Fig. 4 (see also Nof 1983). A heavy lens is situated over a sloping bottom (analogous to β) and propagates with shallow water on its right (i.e., "westward"). It encounters a meridional wall perpendicular to the lens direction of migration. It is intuitively expected that gravity will pull the lens downhill toward deep water (i.e., southward). We shall see, however, that in contrast to this intuitive outcome, the lens actually propagates uphill. From an energy point of view, this bizarre uphill movement of the lens center is possible because it is compensated for by a leakage along the wall, which gradually destructs the ring by draining its fluid.

a. Modeling background

Table 1 summarizes the relevant previous studies of an eddy migration along a free-slip meridional wall.

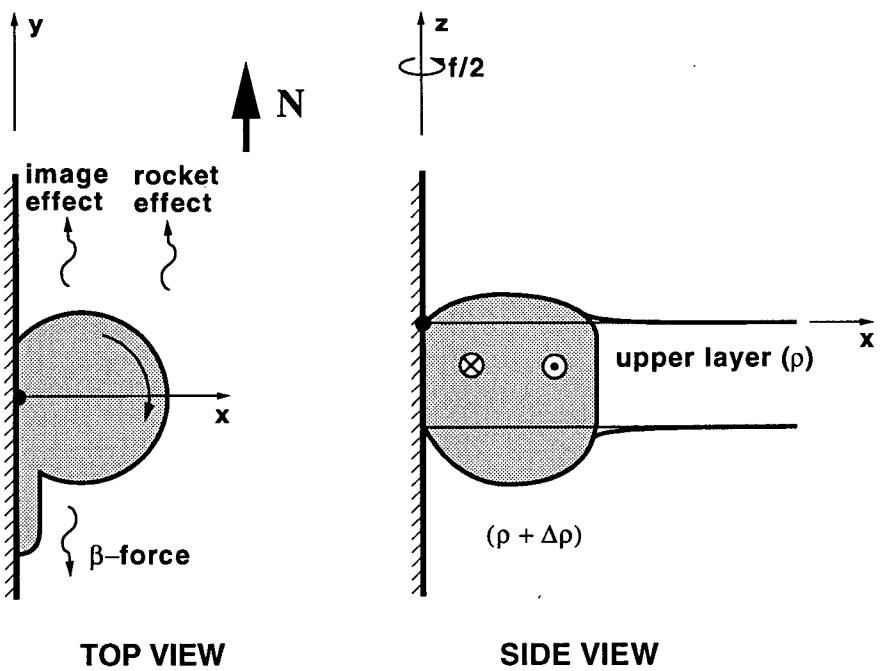

FIG. 3. A schematic diagram of the migration of an eddy above an infinitely deep lower layer next to a wall on a β plane. Three mechanisms determine the migration of an anticyclonic eddy: the image effect and the "rocket" effect try to push an anticyclonic eddy northward, while the β force tends to pull it southward. Our aim here is to find out in which direction the eddy ultimately migrates along a meridional wall. "Wavy" arrows indicate direction of migration.

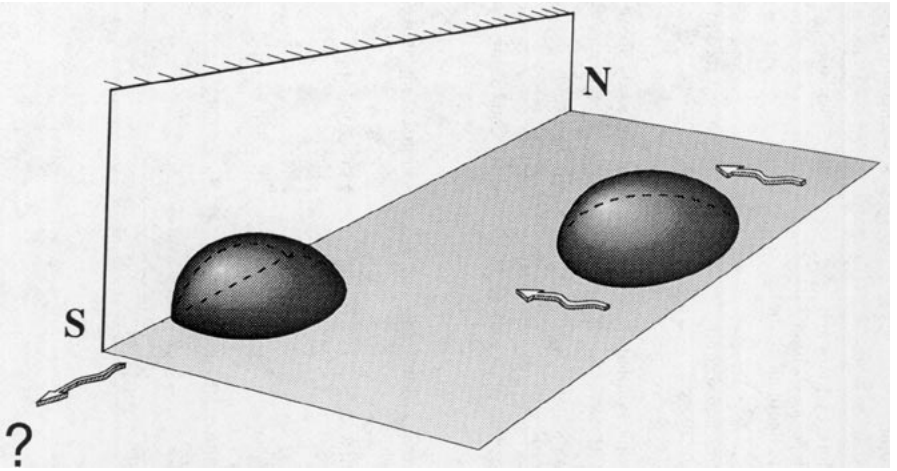

FIG. 4. A schematic diagram of the influence of a meridional wall on the "westward" migration of a bottom lens. In analogy to β, the bottom is sloping in the north–south direction, and the lens initially translates with shallow water on its right (e.g., see Nof 1983). It is intuitively expected that, once the lens encounters the wall, it will start moving downhill (i.e., toward the equator). Surprisingly, however, it turns out that the center of the lens (i.e., the point of maximum pressure) moves uphill due to the image effect and a leakage along the wall (see text). Ultimately, the leakage destroys the lens by completely draining its fluid.

Although all of these studies are informative, they do not directly address the question of lens propagation next to a wall or the combined effect of all alongwall migration mechanisms on eddies with a finite depth along the rim (i.e., nonlenses), which is the focus of our study.

The collisions of an eddy with a sloping bottom topography were investigated by Louis et al. (1982), Louis and Smith (1982), Nof (1983), Smith and O'Brien (1983), Smith (1986), Chapman and Brink (1987), Nakamoto (1989), Smith and Ulrich (1990), Whitehead et al. (1990), Carnevale et al. (1991), and Swaters and Flierl (1991). All of these studies are important because they involve migration speeds equivalent to topographic Rossby waves. However, as we shall see, the topographic effects are not as important as the image effect, which produces much greater migration rates. Note also that the limit of a slope becoming infinite cannot be taken in these studies, therefore, they cannot be used to examine the eddy's migration along a free-slip, meridional vertical wall.

b. *Present study*

The numerical model that we shall use is an isopycnic, primitive equation, two-layer model. This model utilizes a so-called flux corrected transport method for calculating mass flux divergence, which allows us to study strong nonlinear features such as lenslike eddies. The model can be viewed as a stack of shallow fluid layers, each layer with a constant density. The motion within each layer is governed by the shallow-water equations; the layers communicate with each other primarily through the continuity of pressure. An analytical solution is also constructed; it invokes the quasigeostrophic, steady, inviscid, 1½-layer, potential vorticity equation on an f plane.

In section 2 an application of the isopycnic model to lenses reacting to the presence of a wall is considered. As mentioned, we shall see that, contrary to our expectations, the center of these lenses propagates uphill and that the lenses are gradually losing mass via thin jets whose nose propagates downhill. We have chosen to look at lenses first because lenses are the only eddies that are truly isolated in the sense that, in a 1½-layer model, no fluid around them is moving. Hence, even though lenses are highly nonlinear eddies, they are, in a sense, simpler than small amplitude quasigeostrophic eddies, which cannot propagate without affecting the outer fluid.

After completing the analysis of lenses, we shall proceed with analytical analysis and the isopycnic model to examine the reaction of cyclones and anticyclones with a finite depth along the rim (i.e., nonlenses) to the presence of a wall (sections 3 and 4). We shall see that, again, the results are counterintuitive. It turns out that, as the eddies are pressed against the wall, they are transformed into a half-circular (wodon[1]) structure that is fundamentally different from their open-ocean structure. Surprisingly, at the wodon stage the eddies are independent of β even though β is responsible for their generation in the first place. This half-circular (wodon) eddy is also described analytically for quasigeostrophic motions. The results of the analytical so-

[1] The term "wodon" is used because it corresponds to a combination of a *w*all and a m*odon*.

TABLE 1. Summary of previous studies of an isolated eddy's migration along a free-slip meridional wall. Note schematic diagrams at end of table.

Author	Type of model	Mechanism of migration			Type of eddy	
		Image effect	β force	Rocket effect	Description	Configuration
Lamb (1932)	nonlinear, analytical, barotropic	present, discussed	not present	not present	barotropic	See Schematic 1
Masuda et al. (1987), Masuda (1988)	quasigeostrophic, numerical, analytical, f-plane, $1\frac{1}{2}$-layer	present, discussed	not present	not present	baroclinic cyclones and anticyclones with a finite depth along the edge	See Schematic 2
Nof (1988a,b)	quasigeostrophic, analytical, f-plane, barotropic, and $1\frac{1}{2}$-layer	present, not discussed	not present	discussed	as in first and second study above	as in first and second study above
Pierrehumbert (1980)	contour dynamics, barotropic	present, discussed	not present	not present	barotropic (vorticity patch)	as in first study above
Saffman (1979)	nonlinear, analytical, barotropic	present, discussed	not present	not present	barotropic (vorticity patch)	as in first study above
Umatani and Yamagata (1987)	primitive equation, numerical, f-plane, $1\frac{1}{2}$-layer	present, discussed	not present	not present	as in second study above	as in second study above
Wu et al. (1984)	contour dynamics, barotropic	present, discussed	not present	not present	barotropic (vorticity patch)	as in first study above
Yasuda et al. (1986)	quasigeostrophic, numerical, β-plane, $1\frac{1}{2}$-layer	present, discussed	present, not discussed	present, not discussed	as in first study	as in second study above
Present study	quasigeostrophic, primitive equation, analytical, numerical (isopycnic), β-plane, $1\frac{1}{2}$-layer, two-layer	present, discussed	present, discussed	present, discussed	lenses as well as cyclones and anticyclones with a finite depth along the edge	See Schematic 3

Schematic 1

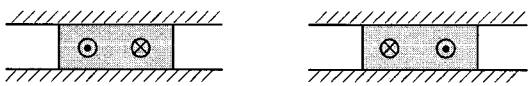

Schematic 2

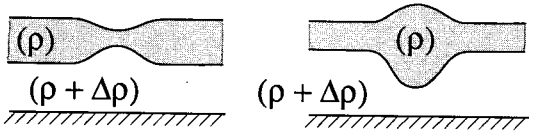

Schematic 3

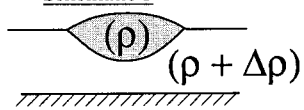

and

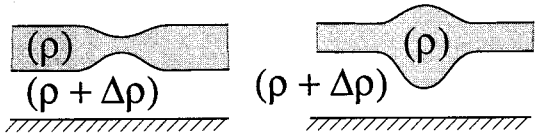

lution will be compared to the numerical results to show that, in the quasigeostrophic limit, the leakages are relatively unimportant. This contradicts the nonlinear (lens) cases where the leakages are of fundamental importance. Finally, the results are applied to various oceanic situations (section 5) and summarized (section 6).

2. The reaction of a lenslike eddy to the presence of a meridional wall

a. General description of the numerical model

In this section, an eddy's migration next to a wall on a β plane is investigated using the isopycnic model of Bleck and Boudra (1986). This primitive equation model may be viewed as a stack of shallow water models. The model consists of two momentum equations, a hydrostatic equation, and a continuity equation:

$$\frac{\partial u}{\partial t} + u\frac{\partial u}{\partial x} + v\frac{\partial u}{\partial y} - fv = -\frac{\partial M}{\partial x} + \frac{\nu}{\Delta p}\nabla(\Delta p \nabla u), \tag{2.1}$$

$$\frac{\partial v}{\partial t} + u\frac{\partial v}{\partial x} + v\frac{\partial v}{\partial y} + fu = -\frac{\partial M}{\partial y} + \frac{\nu}{\Delta p}\nabla(\Delta p \nabla v), \tag{2.2}$$

$$\delta M = p\delta\alpha, \tag{2.3}$$

$$\frac{\partial \Delta p}{\partial t} + \frac{\partial (u\Delta p)}{\partial x} + \frac{\partial (v\Delta p)}{\partial y} = 0, \tag{2.4}$$

where u, v are the zonal and meridional velocity components, Δp is the thickness of a constant density layer, f the Coriolis parameter, M the Montgomery potential, p the pressure, $\delta M = M_{\text{upper layer}} - M_{\text{lower layer}}$, α is the specific volume, $\delta\alpha = \alpha_{\text{upper layer}} - \alpha_{\text{lower layer}}$, ν is the lateral viscosity, and $\nabla = \mathbf{i}\partial/\partial x + \mathbf{j}\partial/\partial y$. The layers communicate vertically through hydrostatically transmitted pressure forces (2.3). Note that there are four unknowns u, v, p, M, and four equations (2.1)–(2.4); therefore, the system is closed.

One of the advantages in Bleck and Boudra's isopycnic model is the use of the so-called flux corrected transport (FCT) technique to solve the continuity equation (2.4) (Zalesak 1979). The FCT method allows isopycnals to outcrop (i.e., $\Delta p = 0$); consequently, it can be used to study very strong nonlinear features such as lenslike eddies.

As shown in Fig. 5, the model consists of a two-layer 1000 km × 1000 km square domain with grid spacing 10 km and time step 10 minutes. Lateral boundary conditions are free slip everywhere. A rigid lid and a flat bottom are chosen as upper and lower boundaries. Velocities are initially (at $t = 0$) in geostrophic balance in the upper layer and at rest below, but due to the nonzero centrifugal force, there is an adjustment after $t = 0$. However, this small imbalance in the initial conditions does not affect the long-term evolution of the ring. For all experiments shown hereafter, the parameters are $f_0 = 10^{-4}$ sec^{-1}, $\beta = 2 \times 10^{-11}$ s^{-1} m^{-1}, $\rho = 1000$ kg m^{-3}, $\Delta\rho = 1$ kg m^{-3}, $g' = 10^{-2}$ m s^{-2}, $\nu = 100$ m^2 s^{-1}, $H \leq 1$ km, and $H_2 = 1000$ km. According to a simple potential vorticity analysis for a flow under the eddy ("bump"), the lower-layer velocity generated by the moving eddy (ΔU) is $\Delta U \sim fR_dH/H_2$, assuming that the horizontal length scale of an eddy is of the same order as the deformation radius. We selected $H/H_2 \leq 0.001$, so that the lower-layer velocity amplitude ($\Delta U \leq 3.16 \times 10^{-3}$ m s^{-1}) is negligible

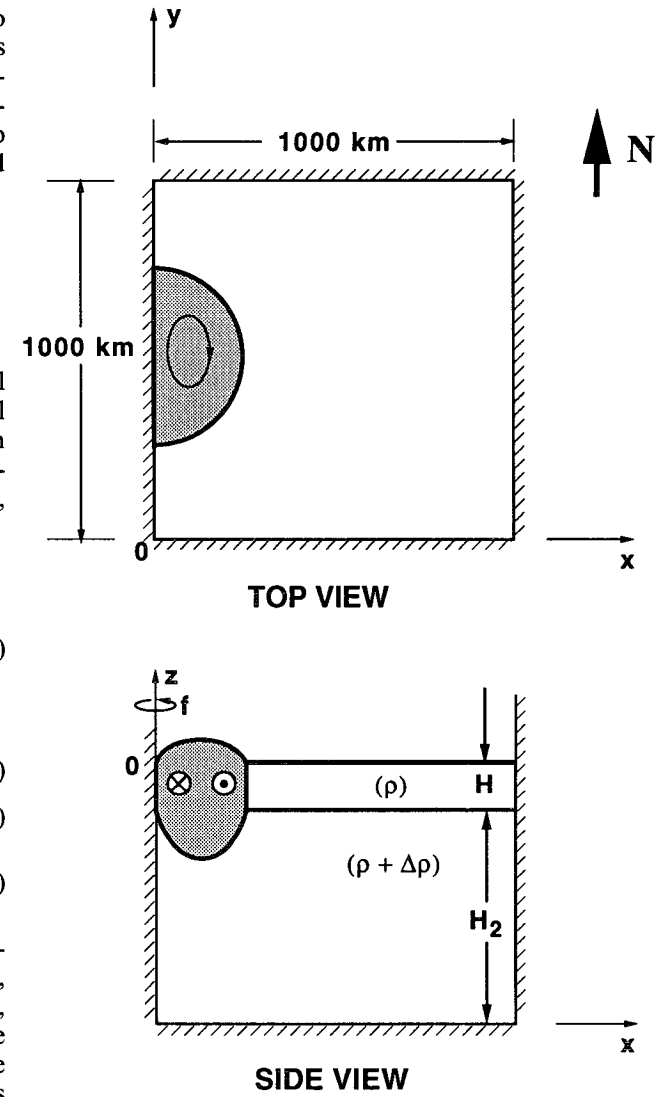

FIG. 5. A schematic diagram of the isopycnic, two-layer, primitive equation model on a β plane. The model is configured in a two-layer, 1000 km × 1000 km square domain with grid spacing 10 km and time step 10 minutes. Lateral boundary conditions are free slip everywhere. A rigid lid and a flat bottom are chosen as upper and lower boundaries. The velocities are initially in geostrophic balance in the upper layer and at rest below.

compared to the upper-layer motion. We shall first study a lens on a β plane.

b. Scaling

Before presenting our numerical runs, it is appropriate to present the scales of the associated parameters. The general scaling presented below is relevant not only for lenses but also for eddies with a finite depth along the rim or quasigeostrophic eddies. The only difference between the two cases is that for lenses the Rossby number is of order unity whereas for the other eddies (with the same length scale) the Rossby number can be small.

1) MIGRATION DUE TO THE β FORCE

For an eddy with a typical azimuthal velocity of $\mathrm{Ro} f_0 R_d$ (where Ro is the Rossby number, which can be of order unity, and R_d is the Rossby radius), β and the presence of the wall are causing an (accelerated) *meridional migration* of $O(\beta R_d^2\ \mathrm{Ro} f_0 t)$ (where t is time) because $\partial v/\partial t \sim O(\beta y u)$. Hence, after a relatively "long" time $[O(\beta R_d)^{-1}]$ the meridional speed is $C_\beta \sim O[\mathrm{Ro}(g'H)^{1/2}]$, which is of the same order as the orbital speed. We shall see shortly that this speed is also of the same order as the migration caused by both the "rocket effect" and the image effect.

2) THE "ROCKET" EFFECT

To illustrate this effect it is recalled that the eddy is pushed toward the wall by β at a westward migration speed of $\sim O(\beta R_d^2)$, it is assumed that the width of the leakage is $O(\beta R_d^2/f_0)$. After a long time $[O(1/\beta R_d)]$, the generated leakage along the wall has a length $\sim O(\mathrm{Ro} f_0/\beta)$, and a height $\sim O(H)$; therefore, the leaked volume is $\sim O(\mathrm{Ro} H R_d^2)$. Since the speed in the leakage is $O[\mathrm{Ro}(g'H)^{1/2}]$, the leakage has a momentum of $\sim O[\mathrm{Ro}^2 H R_d^2 (g'H)^{1/2}]$. If the migration speed produced by the leakage is denoted by C_{rocket}, then the eddy's momentum is $\sim C_{\mathrm{rocket}} H R_d^2$ and by conservation of momentum, we obtain

$$C_{\mathrm{rocket}} \sim O[\mathrm{Ro}^2 (g'H)^{1/2}],$$

which, for $\mathrm{Ro} \sim O(1)$, is of the same order as the drift due to β but is always pointing in the opposite direction.

3) THE IMAGE EFFECT

The migration speed due to the image effect (i.e., due to the fact that there can be no flow into the wall) is of the same order as the orbital speed,

$$C_i \sim O[\mathrm{Ro}(g'H)^{1/2}],$$

because at $t > (\beta R_d)^{-1}$ the eddy is forced into the wall a distance of $O(R_d)$. It is now clear that C_i is of the same order as the β-induced drift along the wall. For $\mathrm{Ro} \sim O(1)$ both speeds are also of the same order as the "rocket" speed.

That, for $\mathrm{Ro} \sim O(1)$, all of the three migration tendencies are of the same order, $(g'H)^{1/2}$, shows that it is impossible to tell in advance in which direction the eddy will move as a result of its impact with the wall. We shall see that all of our experiments show that the image effect dominates even though the other two effects are of similar order of magnitude. Of particular surprise is the lens case, which is expected to be dominated by the β force (i.e., the eddy is expected to go downhill as shown in Fig. 4) and yet is dominated by the image effect.

Note that the meridional open-ocean migration due to Rossby wave radiation (e.g., see McWilliams and Flierl 1979) is usually much smaller than our long-wall drift. Even if the open ocean meridional speed is taken to be as high as $O(\beta R_d^2)$, it is still usually small compared to $\mathrm{Ro}(g'H)^{1/2}$. The ratio between the two speeds is $\beta R_d/(f_0 \mathrm{Ro})$, which, even for quasigeostrophic eddies [$\mathrm{Ro} \sim O(0.1)$], is of $O(10^{-1})$. In view of this, we ignore the meridional drift due to Rossby wave radiation. Similarly, the meridional migration induced by topographic Rossby waves $\{\sim O[S(g'H)^{1/2}]$, where S is the bottom slope, typically 10^{-2} or $10^{-3}\}$ is also small compared to the image induced speed $[\mathrm{Ro}(g'H)^{1/2}]$ because the eddys Rossby number $[\sim O(0.1)]$ is typically larger than the bottom slope.

c. Numerical study of a Gaussian lenslike eddy near a wall

In this subsection, we examine the β force, the "rocket," and the image effect on a lenslike eddy. The results of a typical run are shown in Fig. 6, which illustrates that, in contrast to our intuition that the lens will go "downhill" (i.e., southward) once it reaches the wall, the ring moves "uphill" (i.e., northward). This indicates that of the three migration mechanisms, the image effect is the most dominant one. From an energy conservation point of view, the surprising uphill movement is possible because of the near-wall leakage, which is related to Kelvin wave propagation. It is apparent from Fig. 6 that the leakage is directed southward so that the center of mass (of the lens and leakage) does not, in fact, move northward (or uphill) and energy is conserved. The above experiment illustrates how crucial the leakage is for the lens–wall interaction process. Without it the lens could not have been dominated by the image effect. Note that the lens average migration speed along the wall is 0.4 km day^{-1}, much smaller than that of the quasigeostrophic eddies discussed below.

3. Analytical study of a quasigeostrophic eddy along a wall on an f plane

In contrast to the previous section where highly nonlinear eddies were examined, we shall now study

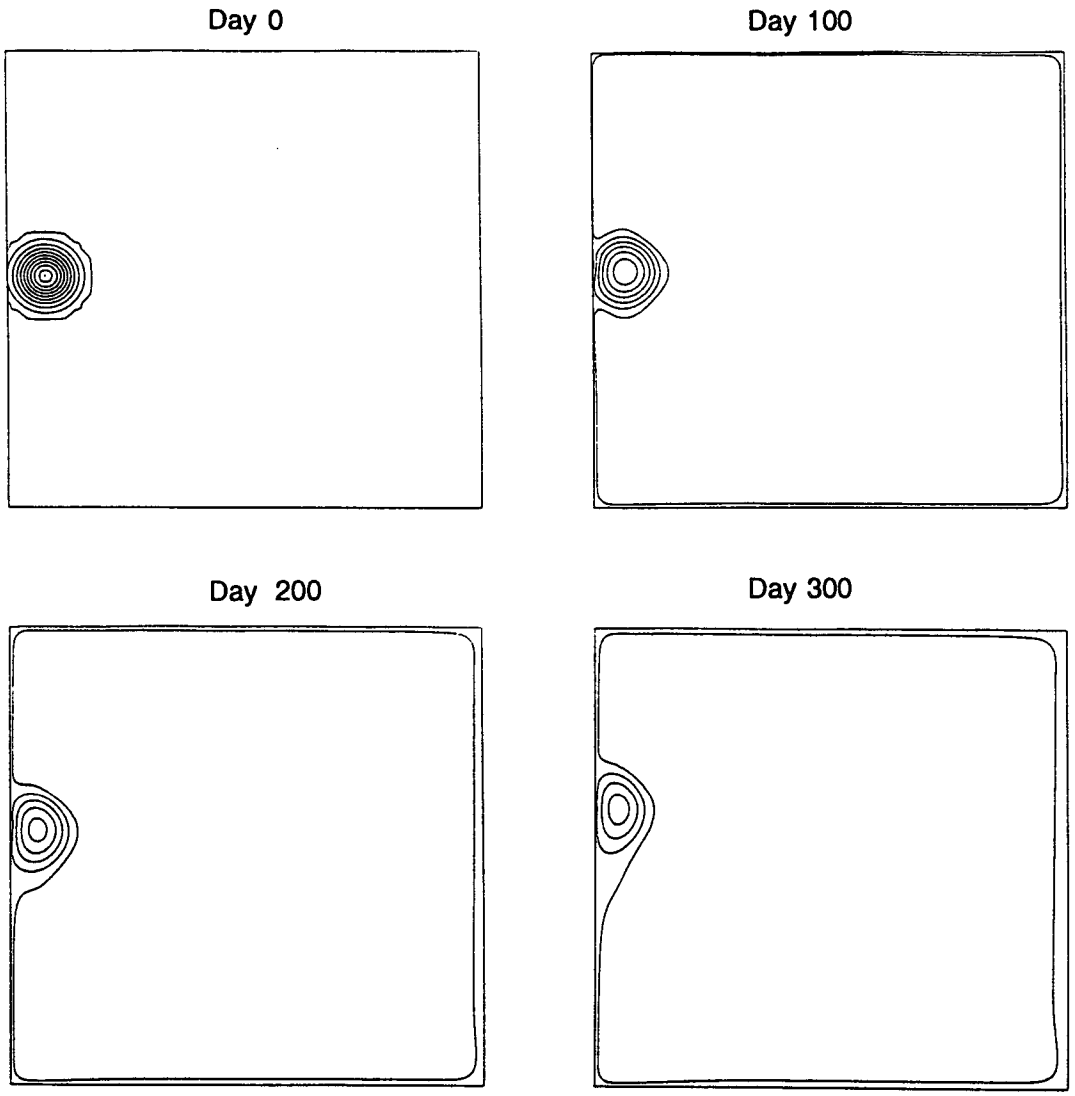

FIG. 6. Contours of the interfacial displacement anomaly for a Gaussian lenslike eddy on a β plane. The maximum potential vorticity anomaly (in s^{-1} m^{-1}) is -7.7×10^{-8} and the deformation radius is 25 km. The average migration speed along the wall is about 0.1 km day^{-1}, much smaller than the alongwall drift of quasigeostrophic eddies (about 4 km day^{-1}), which will be discussed later (section 3). This difference in speeds is probably due to the presence of the β force, which opposes the image effect and pulls the lens southward. The parameters are $H = 0$ m, $H_n = 625$ m, $x_c = 100$ km, $y_c = 500$ km, and the radius of maximum orbital speed of the Gaussian eddy is $R = 50$ km. The contour interval is 62.5 m.

a half-circular, inviscid, quasigeostrophic eddy migrating along a wall on an f plane (Fig. 7). As before, we use a 1½-layer model; while the infinitely deep lower layer is motionless, the upper layer has two active regions: the interior (i.e., the ring) and the exterior. The ring is bounded by a half-circle with a radius $r = a$ on the right and the wall on the left. We shall see that, as a result of the image effect, which again dominates the flow, the eddy migrates *steadily* along the wall. We shall also see that, although our present study does not involve β, it is quite relevant to the general problem where β *is* present. This is so because there is a "window" of time $[(\beta R_d)^{-1} < t < (\mathrm{Ro}\beta R_d)^{-1}]$ for which the behavior of an eddy next to a wall on a β plane does not differ much from that of an eddy next to a wall on an f plane.

The wodon solution presented below is very similar to the modon solution of Flierl et al. (1980) except that it addresses a single f-plane vortex next to a wall rather than a zonally moving modon (i.e., double vortex) on a β plane. The importance of our present solution is not in its mathematical details (which are not new) but rather in the recognition that *any midocean vortex on a β plane will be ultimately converted into*

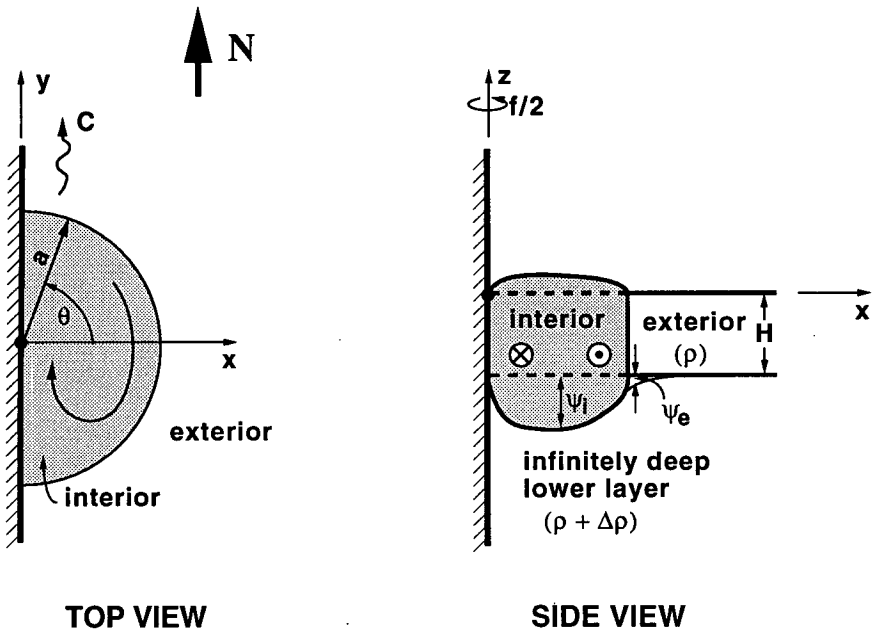

FIG. 7. A schematic diagram of an eddy migrating at a constant speed (C) along a wall on an f plane. While the infinitely deep lower layer is motionless, the upper layer has two active regions: the interior (i.e., the ring) and the exterior. The ring is bounded by a free streamline at $r = a$ and the wall. As a result of the image effect, the eddy steadily migrates along the wall. Note that H is the undisturbed depth of the upper layer. As before, a wavy arrow indicates migration.

such an f-plane wodon once it completes its adjustment to the presence of a meridional wall. There is some unavoidable overlap between the mathematical details presented below and the solution of Flierl et al. (1980) because an attempt has been made to make the present paper self-contained.

a. Governing equations

The time-dependent quasigeostrophic governing equation in dimensional form is

$$[\partial/\partial t + g'/fJ(\psi,)][\nabla^2\psi - \psi/R_d^2] = 0, \quad (3.1)$$

where J is the Jacobian operator, ψ the interfacial displacement anomaly measured positively downward in a stationary coordinate system, R_d the Rossby deformation radius, and H the undisturbed upper-layer thickness (e.g., Pedlosky 1987). If we assume that the eddy steadily migrates along a wall at a speed C, then we can rewrite (3.1) by replacing the time derivative $\partial/\partial t$ with $-C\partial/\partial y$. This gives

$$\nabla^2\psi - \psi/R_d^2 = F(\psi - fCr\cos\theta/g'), \quad (3.2)$$

where ψ is now the interfacial displacement anomaly measured positively downward in polar coordinates (r, θ) moving at a constant speed C, and F is an arbitrary function of $[\psi - fCr\cos\theta/g']$. Note that a free streamline divides the studied area into two regions: an interior and an exterior. We shall now derive the governing equations for both the interior and the exterior.

For the exterior ($r > a$), the value of F on any line of constant $(\psi - fCr\cos\theta/g')$ is determined from the far-field condition, which states that all interfacial displacement anomalies vanish since the eddy is isolated; that is, $\psi \to 0$ as $r \to \infty$. Therefore, (3.2) becomes

$$\nabla^2\psi_e - \psi_e/R_d^2 = 0, \quad (3.3)$$

where the subscript e associates the corresponding variable with the exterior. Equation (3.3) states that the potential vorticity anomaly of the exterior is zero.

In the interior ($0 \leq r \leq a$), it is assumed that F is a linear function of $(\psi - fCr\cos\theta/g')$,

$$F(\psi_i - fCr\cos\theta/g') = -(\psi_i - fCr\cos\theta/g')/L^2, \quad (3.4a)$$

where L is a constant with a dimension of length, and the subscript i denotes association with the interior. Under such conditions, (3.2) becomes

$$\nabla^2\psi_i + \frac{k^2}{a^2}\psi_i = \left(\frac{k^2}{a^2} + \frac{1}{R_d^2}\right)\frac{fC}{g'}r\cos\theta, \quad (3.4b)$$

where k, the eigenvalue of the wodon to be determined, is given by $a(1/L^2 - 1/R_d^2)^{1/2}$.

b. Boundary conditions

As mentioned, the eddy is bounded by the wall on the left (looking northward) and the perimeter of the half circle on the right. The boundary conditions are

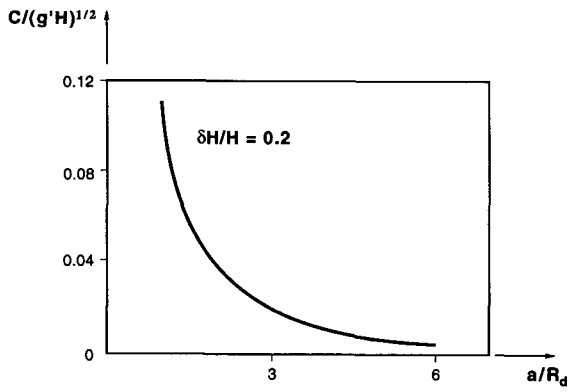

FIG. 8. The image-induced migration speed C as a function of the radius of the wodon a. It demonstrates that the larger the wodon's radius, the smaller the migration speed.

$$\psi_e = \psi_i = fCa\cos\theta/g'; \quad r = a \tag{3.5}$$

$$\partial\psi_e/\partial r = \partial\psi_i/\partial r; \quad r = a \tag{3.6}$$

$$\psi_i = \psi_e = 0; \quad \theta = \pm\pi/2 \tag{3.7}$$

$$\psi_e \to 0; \quad r \to \infty, \tag{3.8}$$

where the first condition (3.5) reflects the continuities of the pressure and the potential vorticity across the eddy's edge. [The continuity of the potential vorticity can be seen by substituting (3.5) into (3.2).] The second condition (3.6) implies that the tangential speed is continuous along the eddy's edge and the third condition (3.7) states that no mass transport penetrates the wall. The last condition (3.8) states that the eddy is isolated.

c. Solution

To solve this problem of coupling an eddy with its exterior, we first need to find a general solution for the eddy and another solution for the exterior. The method of the separation of variables is used to obtain general solutions for both the interior and the exterior. Then, we match these two general solutions along the eddy's edge and thus obtain the desired detailed solution.

The solution of (3.3) and (3.4) satisfying (3.5)–(3.8) is

$$\psi_i = \delta H\cos\theta\left[|J_1(k)|\,\frac{r}{a}\left(\frac{kR_d}{a}\right)^2 + |J_1(k)|\,\frac{r}{a} + J_1\left(k\,\frac{r}{a}\right)\right] \tag{3.9}$$

$$\psi_e = \delta H\cos\theta\,|J_1(k)|\left(\frac{kR_d}{a}\right)^2\frac{K_1(r/R_d)}{K_1(a/R_d)} \tag{3.10}$$

$$C = \frac{g'^2}{f^3}\,\frac{H\delta H}{a^3}\,k^2|J_1(k)| \tag{3.11}$$

$$\frac{k|J_1(k)|}{|J_2(k)|} = \frac{K_1(a/R_d)}{K_2(a/R_d)}\,\frac{a}{R_d}, \tag{3.12}$$

where $J_n\,(n = 1, 2)$ are the Bessel functions of the first kind, $K_n\,(n = 1, 2)$ are the modified Bessel functions of the second kind, and the parameter (δH) is given by

$$\delta H = H_m\Big/\left[|J_1(k)|\,\frac{d}{a}\left(\frac{kR_d}{a}\right)^2 + |J_1(k)|\,\frac{d}{a} + J_1\left(k\,\frac{d}{a}\right)\right], \tag{3.13}$$

where H_m is the maximum interfacial displacement anomaly, and d is the horizontal distance between the extreme of the interfacial displacement anomaly and the wall. Next, we determine the distance (d) by finding the root of $\partial\psi_i/\partial r = 0$ at $\theta = 0$,

$$J_2(kd/a) - J_0(kd/a) = 2|J_1(k)|[k(R_d/a)^2 + 1/k], \tag{3.14}$$

where k is the eigenvalue of the problem; for a wodon's structure shown in Fig. 7, k is given by the smallest root of (3.14).

TABLE 2. Wodonlike eddy calculations.

Eddy type	Cyclonic (Fig. 9)	Anticyclonic (not shown)
	Parameters	
Undisturbed upper-layer thickness (H)	1000 m	1000 m
Maximum potential vorticity anomaly (q'_m)	9.8×10^{-8} sec^{-1} m^{-1}	-4.4×10^{-8} sec^{-1} m^{-1}
Deformation radius (R_d)	31.6 km	31.6 km
Wodon's radius (a)	150 km	150 km
	Results	
Migration direction	southward	northward
Numerical migration speed (averaged)	−4.3 km day^{-1}	5.2 km day^{-1}
Analytical migration speed	−5.0 km day^{-1}	5.0 km day^{-1}
Migration speed relative error	14%	4%

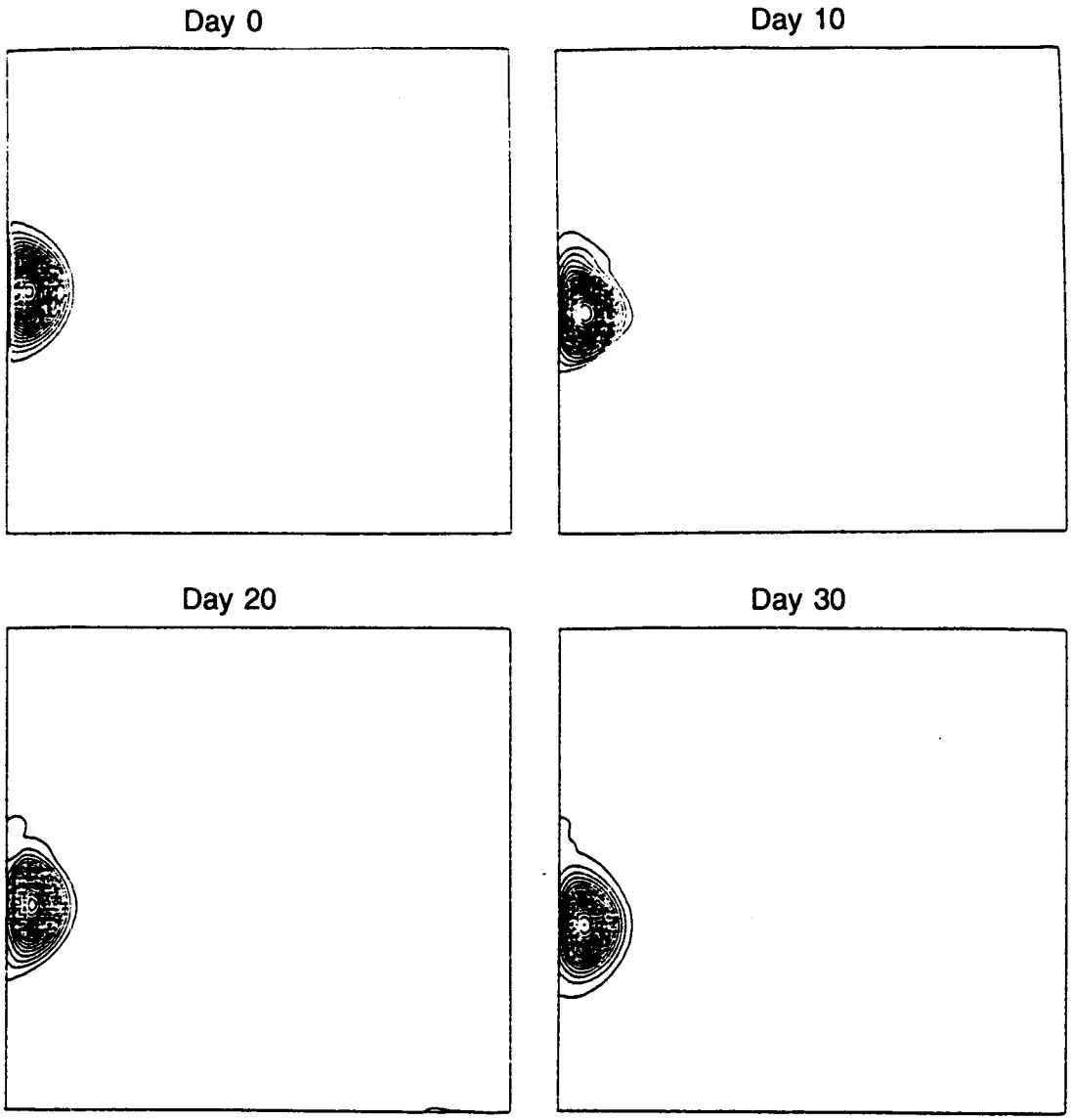

FIG. 9. Contours of the potential vorticity anomaly for a cyclonic wodon on an f plane. It shows that the cyclonic wodon moves southward at a constant speed of 4.3 km day^{-1}. The parameters are $H = 1000$ m, $q'_m = 9.8 \times 10^{-8}$ s^{-1} m^{-1}, and $a = 150$ km. The contour interval is 5×10^{-9} s^{-1} m^{-1}.

d. Properties of the solution

In the wodon solution, when $H_m > 0$ (i.e., $\psi > 0$), then $C > 0$; that is, an anticyclone migrates northward. Similarly, when $H_m < 0$ (i.e., $\psi < 0$), then $C < 0$; that is, a cyclone migrates southward. As there is no leakage nor β in the problem at hand, the migration pattern corresponds to the image effect. From relations (3.11) and (3.13), it is clear that the migration speed (C) is linearly proportional to the maximum eddy interfacial displacement anomaly (H_m) and that the speed (C) increases as the undisturbed depth (H) increases. The migration speed decreases with an increasing Coriolis parameter (f) and radius (a) because $k^2|J_1(k)|$ increases more slowly than a^3. Figure 8 shows the migration speed as a function of the radius according to (3.11) for a fixed $\delta H/H$.

Two comments should be made before completing the present discussion. First, it is difficult to recognize the fundamental importance of our wodon solution at this stage. This will become apparent in the next section where it will be demonstrated that the modon solution compares extremely well with numerical runs of eddies on a β plane. In other words, as already mentioned, the importance of the *modon solution stems from the fact that open-ocean eddies tend to convert to it once they respond to the presence of the wall.* Second, it should be pointed out that Lamb's dipole solution

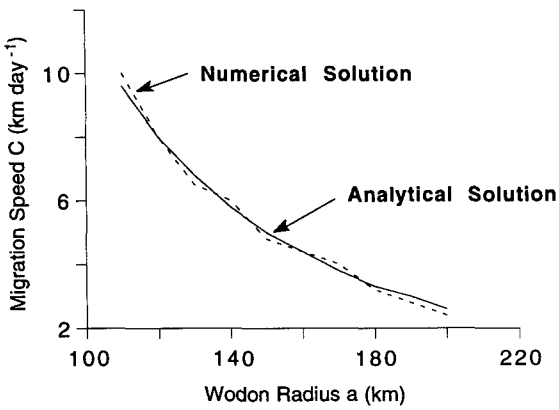

FIG. 10. The migration speed as a function of the wodon radius for an anticyclonic wodon. Note that the analytical solution (solid line) agrees with the numerical solution (dashed line) within an error of 10%.

(1932) for a barotropic vortex is recovered from (3.9)–(3.12) when we take the limit of $R_d \to \infty$, as should be the case.

4. Numerical studies of eddy reaction to the presence of a wall on a β plane

a. *Verification of the isopycnic model using the wodon solution*

Before addressing the general eddy–wall problem, it is appropriate to test the isopycnic model using the wodon solution (3.9)–(3.12). Here, we start with a half-circular eddy next to a wall on an f plane and compare the analytical and numerical migration rates. Later on, for the most general problem, we will start with an eddy initially situated in the middle of a β plane ocean. Table 2 lists the parameters and results of such a numerical experiment. Contours of the potential vorticity anomaly $[(q' \equiv f_0 + \partial v/\partial x - \partial u/\partial y/\Delta p - f_0/H]$ for a cyclone are shown in Fig. 9. As expected, contours of potential vorticity anomaly for an anticyclone (not shown) are very close to those of Fig. 9 because the analytical solution is quasigeostrophic and the associated numerical runs are close to being quasigeostrophic as well.

Calculation of the migration speed (given in Table 2) shows that the analytical solution agrees with the numerical one within a relative error of 14%. Figure 10 shows numerically and analytically calculated migration speeds as a function of the anticyclonic wodon's radius. To obtain Fig. 10, we rerun the earlier case with the wodon radius (a), which varies from 100 km to 200 km with an increment of 10 km. It again demonstrates that, for an anticyclonic wodon, the numerical results agree with the analytical calculation within a relative error of 10%. Therefore, we can conclude that the isopycnic model works correctly. We note that the relative error of the migration speed for the cyclone (14%) is much larger than that for the anticyclone (4%). We use different values for a, H, and H_m to reconfirm the above asymmetry between the cyclone and the anticyclone. The asymmetry is probably due to the ageostrophic components, which make cyclones less stable and more dispersive than anticyclones (Williams and Yamagata 1984). Such a dispersion tendency will prevent the initial (numerical) cyclonic eddies from maintaining their structure and shape throughout the migration processes. Hence, they are expected to deviate more from the steady (nondispersive) analytical solution.

Note that, in contrast to the lens, our quasigeostrophic wodon does not leak much fluid along the wall. This is consistent with our scaling analysis (section 2b), which showed that both the leaked volume $[\sim O(\mathrm{Ro} HR_d^2)]$ and the alongwall migration due to the rocket effect $\{\sim O[(\mathrm{Ro}^2(g'H)^{1/2}]\}$ increases with nonlinearity implying that the leakage is less important for small Rossby number flows.

b. *Numerical study of a Gaussian eddy with finite undisturbed depth along its edge*

Encouraged by the analytical verification of the numerical model presented earlier in section 4a, we shall

TABLE 3. Calculation of Gaussian eddy migration ($f_0 = 10^{-4}$ sec^{-1}, $\beta = 2 \times 10^{-11}$ sec^{-1} m^{-1}).

Eddy type	Cyclonic (Fig. 11a)	Anticyclonic (Fig. 12a)
Parameters		
Undisturbed upper-layer thickness (H)	625 m	625 m
Maximum potential vorticity anomaly (q'_m sec^{-1} m^{-1})	2.1×10^{-7}	-7.8×10^{-8}
Maximum speed radius (R)	50 km	50 km
Deformation radius (R_d)	25 km	25 km
Results		
Migration direction	southward	northward
Numerical migration speed (C_{num})	−5.0 km day^{-1}	6.7 km day^{-1}
Analytical migration speed (C)	−6.1 km day^{-1}	6.1 km day^{-1}
Migration speed relative error ($\lvert C_{num} - C\rvert/\lvert C\rvert$)	18%	9%

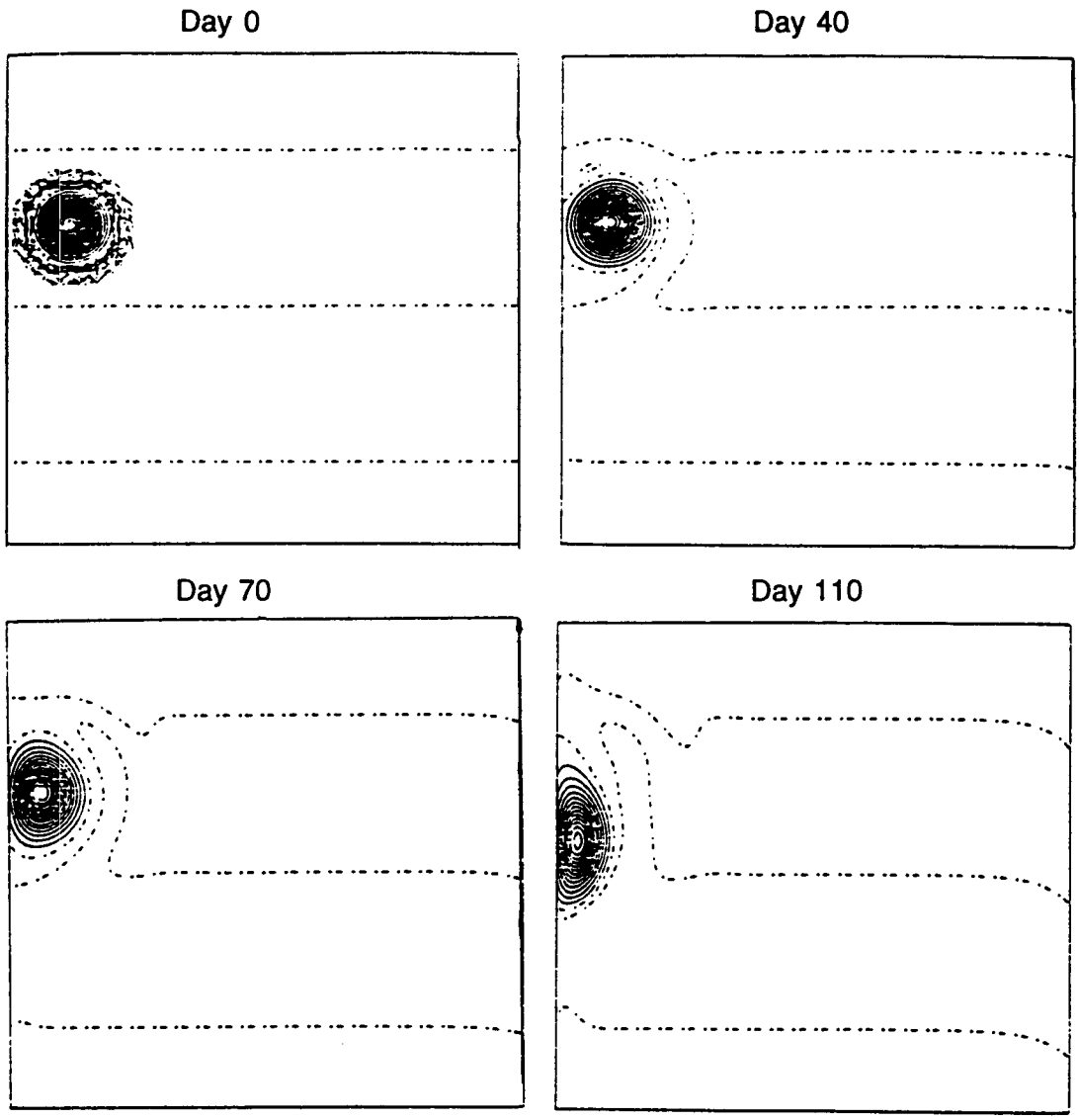

FIG. 11a. Contours of the potential vorticity anomaly for the general problem of a Gaussian cyclonic eddy on a β plane. The β drift keeps pushing the eddy toward the wall and transforms the originally circular eddy into a wodon, which is a new equilibrium state. After the transformation is completed, the wodon propagates to the south. The parameters are H = 625 m, $q'_m = 2.1 \times 10^{-7}$ s^{-1} m^{-1}, x_c = 130 km, y_c = 650 km, R = 50 km. The contour interval is 10^{-8} s^{-1} m^{-1}. As discussed in the text, for the time "window," $(\beta R_d)^{-1} < t < (\mathrm{Ro}\beta R_d)^{-1}$, β is not important.

now proceed to the general eddy–wall problem where we begin our runs with an eddy *away* from the wall.

To do so, we specify the initial Gaussian upper layer to be

$$\Delta p = \begin{cases} H + H_m \exp\{-[(x - x_c)^2 \\ \qquad + (y - y_c)^2]/2R^2\}, & 0 \leqslant r \leqslant 2R \\ H, \quad \text{otherwise}, \end{cases} \tag{4.5}$$

where H is the undisturbed upper-layer thickness, H_m the maximum interfacial displacement anomaly, (x_c, y_c) describe the position of the eddy's mass center, and R is the radius at which the tangential speed reaches its maximum value.

Table 3 lists the parameters and results of each numerical experiment. Figure 11a shows contours of the potential vorticity anomaly q' [again $q' \equiv (f_0 + \beta y + \partial v/\partial x - \partial u/\partial y)/\Delta p - f_0/H$] for the Gaussian cyclonic eddy. At $t = 0$, the western edge of the circular eddy is 30 km away from the western wall. Due to the β drift, the eddy migrates westward toward the wall. (Note that the β drift, i.e., the eddy's westward migration due to the β effect, is different from the term "the β force," which is related to a meridional migration of

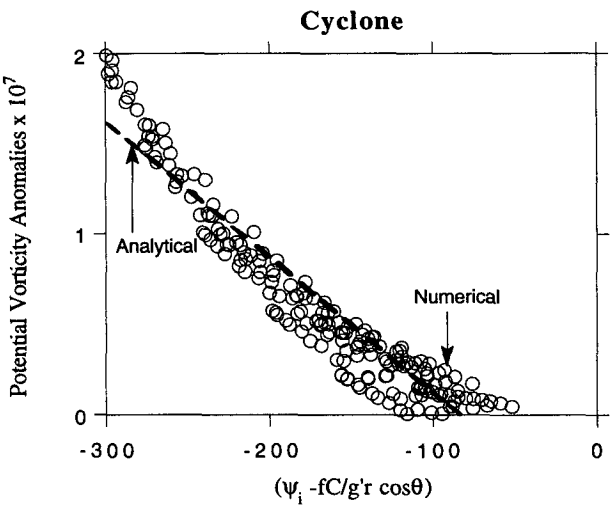

FIG. 11b. A scatterplot of potential vorticity anomalies inside the cyclonic eddy as a function of $(\psi_i - fC/g'r\cos\theta)$ on day 110.

an eddy along a wall.) As the eddy is forced against the wall, its shape is distorted and, in addition to its gradually slowing westward migration, it begins to migrate southward along the wall. After its westward migration is completely arrested by the wall, the original circular eddy is transformed into a wodon. This wodonlike eddy steadily migrates southward along the wall. Using the wodon solution (3.11), the wodon's migration speed is analytically calculated and compared with the numerically calculated speed (see Table 3). Table 3 illustrates that the f-plane wodon analytical speed agrees well with the β-plane numerical speed, implying that, at least for the time window mentioned earlier, β plays a small role in the eddy's migration along the wall. This last result regarding the independence of β was also found by Yasuda et al. (1986), who used a (nonisopycnic) quasigeostrophic model.

The important ingredients of the eddy–wall collisions can now be reiterated as follows. First, the β drift keeps pushing the eddy against the wall. After the eddy adjusts to the wall [$t \geq (\beta R_d)^{-1}$, corresponding to the length of the eddy, R_d, divided by the westward migration βR_d^2], the eddy's westward migration is completely arrested. A combination of the arresting effect of the wall and the β drift transforms the circular eddy into a wodon. Then, the wodon propagates along the wall as if β is no longer present until the change in latitude that the eddy experiences is so great that its relative vorticity is significantly altered [$t > (\mathrm{Ro}\beta R_d)^{-1}$, corresponding to the length of the basin $L \sim O(f/\beta)$ divided by the migration rate $\sim O(\mathrm{Ro}fR_d)$ where Ro is the Rossby number]. It implies that for the "window" of time mentioned above we can analytically calculate the eddy's alongwall migration speed on a β plane using the f-plane wodon formula (3.11).

To support this important point, we design the following numerical experiments. We use data of day 110, corresponding to a mature eddy–wodon, to restart the program but let $\beta = 0$. After it runs from day 110 to day 180, we compare the above two results. It is found that, between day 110 and day 130, both runs give similar numerical migration speeds of 5.0 km day^{-1} with a relative speed difference of 10%. Our numerical calculation also shows that later on, from day 130 to day 180, when the wodon moves southward far away from its original latitude [i.e., $t > (\mathrm{Ro}\beta R_d)^{-1}$], the wodon with β moves faster than that without β. As mentioned, this is so because, as the wodon moves farther to the south, the variation of the planetary vorticity eventually becomes of the same order of magnitude as the relative vorticity and, consequently, it is no longer negligible. For instance, in Fig. 11a, $\zeta \sim 2 \times 10^{-5}$ sec^{-1} and $\beta \sim 2 \times 10^{-11}$ sec^{-1} m^{-1}, so that $\zeta/\beta \sim 1000$ km, and the wodon solution is valid as long as it has migrated much less than 1000 km away from its original latitude.

As an additional comparison between the analytical and the numerical experiments, we calculated the potential vorticity anomalies inside the eddy as a function of $(\psi_i - fC/g'r\cos\theta)$ for the cyclonic eddy shown in Fig. 11a at day 110, and for the anticyclonic eddy shown in Fig. 12a at day 80. This is shown in the scatterplots (Figs. 11b and 12b), both of which imply a linear relationship between the numerical potential vorticity anomalies and $(\psi_i - fC/g'r\cos\theta)$, which, in turn, means that a Gaussian eddy has indeed been converted into a wodon. Such a conversion into a wodon cannot, of course, be complete due to the presence of small friction and dispersion in the numerical model. The cyclonic scatter in Fig. 11b is greater than the anticyclonic scatter of Fig. 12b and this is in agreement with our previous discussion regarding the stronger dispersion of cyclonic eddies. It is also worth noting that a potential vorticity tongue usually wraps around the eddy (Figs. 11a and 12a). The amplitude of the tongue is very weak compared with that of the eddy, and, therefore, its effect on the eddy is very small. As an additional test of the numerical model, we placed the eddy at the center of the basin (instead of next to the wall) and reran the case as shown in Fig. 11. We found that, although the details of the offshore migration were, of course, different, the final alongwall migration was similar to the one presented above.

Three additional comments should be made before concluding the present discussion. First, as shown in relation (4.5), our initial pressure field has a small step as one crosses $r = 2R$. To check the effect of this step on the migration of an eddy, we reran the case of Fig. 12a with a continuous Gaussian profile. We found that, except for a small change in the initial adjustment process, the case with a small step gives a very similar result to that of the continuous Gaussian profile. Hence, this discontinuity has a minimum effect on an eddy's migration process.

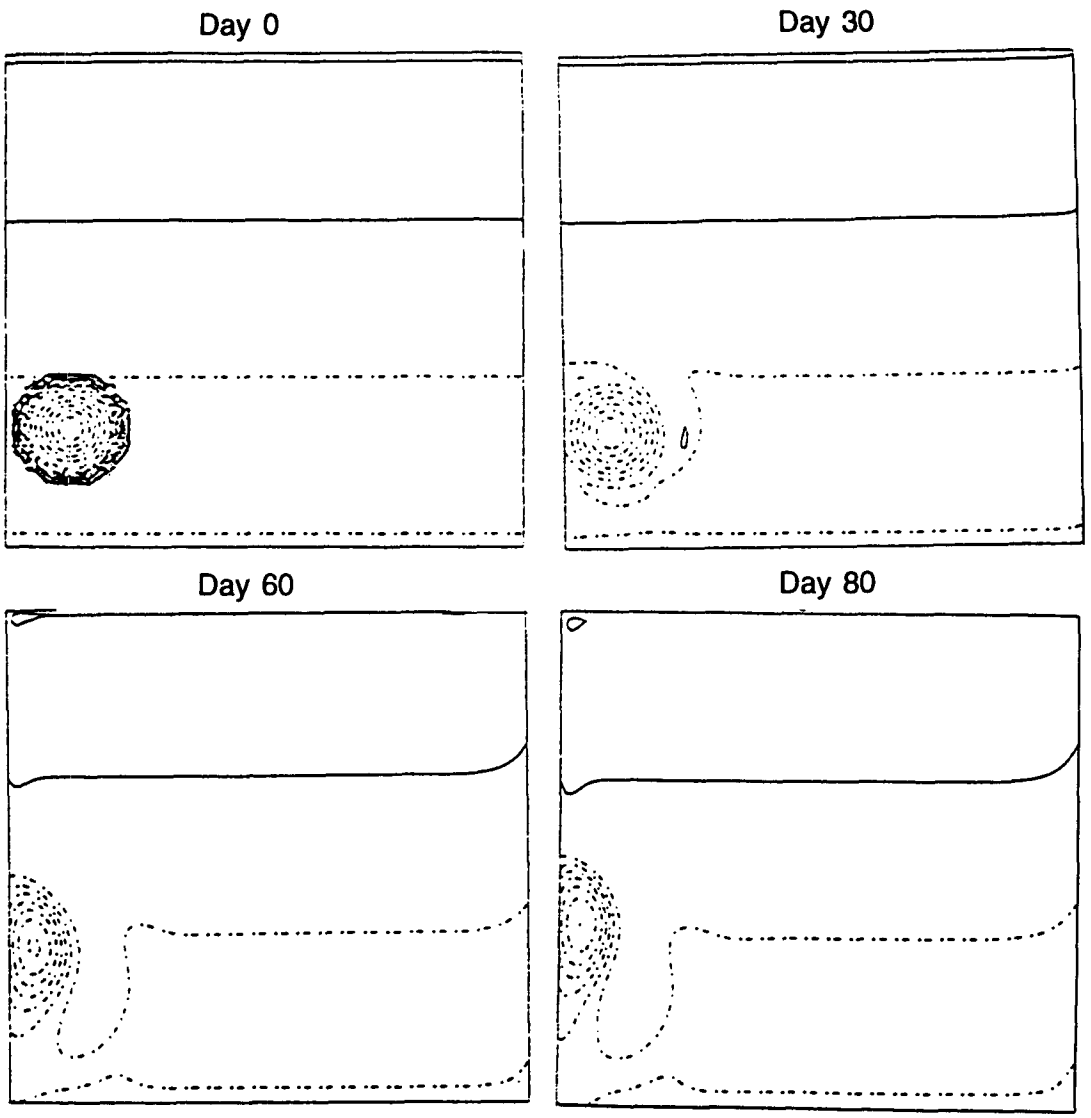

FIG. 12a. As in Fig. 11a except for an anticyclonic eddy. The parameters are $H = 625$ m, $q'_m = -7.8 \times 10^{-8}$ sec^{-1} m^{-1}, $x_c = 130$ km, $y_c = 250$ km, $R = 50$ km. The contour interval is 10^{-8} sec^{-1} m^{-1}.

Second, one may wonder how sensitive is the isopycnic model to the spatial grid size (Δx and Δy). To investigate this point, we ran the case of Fig. 9 using $\Delta x = \Delta y = 5$ km, 10 km, and 20 km. We found that the migration speed of an eddy is not very sensitive to choices of the grid size. In particular, the results from $\Delta x = 5$ km are almost identical to those of $\Delta x = 10$ km.

Third, the quasigeostrophic eddies migrate along the wall about ten times faster than the lens probably due to a stronger southward β force that almost cancels the lens' rocket and image effect.

5. Possible applications

A detailed comparison of our models with observations is very difficult at this stage because of the limited available data and the simplifications made in our models. Therefore, only a qualitative comparison is possible. We shall discuss three observations; the first two support the results of our theory, while the last one neither supports nor rejects our analysis.

The first observation supporting our model's results is provided by Hamon (1965). He investigated southern Pacific rings shed by the East Australian Current, using the results of eight cruises from 1960 to 1964. Anticyclonic eddies about 250 km in diameter were found near the eastern Australian continental shelf in 35°E. These rings moved poleward at a speed of about 4 km day^{-1}. The second observation, which was already mentioned in the Introduction (Kirwan et al. 1988), made by satellite-tracked drifters, studied two rings shed by the Loop Current in 1980 and 1982. Both

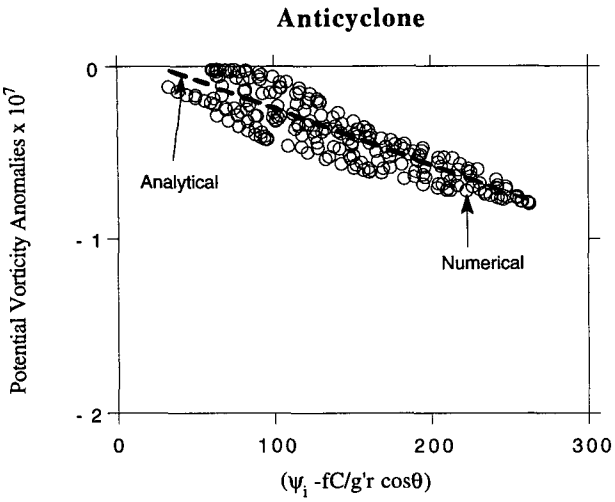

FIG. 12b. A scatterplot of potential vorticity anomalies inside the anticyclonic eddy as a function of ($\psi_i = -fCg'r\cos\theta$) on day 80.

rings encountered the Mexican continental slope at 22.8°N, 95.5°W. After both rings underwent an adjustment process, they maintained a vortex character for several months in the slope region and migrated slowly northward at a speed of 3.5 km day^{-1} (Fig. 2). Fig. 2 also shows that both eddies returned to the south when they left the coast.

While the direction and magnitude of the migration speeds in the above two observations are the same as those given by our models, it is appropriate to point out that there are some other observational studies that may indicate a different kind of behavior. For example, Evans et al. (1985) constructed a chronology of warm core ring 82B from satellite-derived thermal imagery and showed that this anticyclonic ring migrated westward and then southwestward at a speed of 3 km day^{-1} (Fig. 1). This observation can be reconciled with our study in two different ways. First, Cornillon et al. (1989) argue that such rings move southward because they are constantly interacting with other flows. They suggest that once the rings are free from such interactions their movement is toward the northwest rather than the southwest. Second, since the warm core ring of Fig. 1 stayed quite far away from the continental slope, it is expected that our image effect would be very weak. As Flierl (1984) proposed, it is quite possible that the combination of the westward β drift and radiated Rossby waves drag caused it to translate southwestward rather than northeastward.

6. Summary

Both a 1½-layer analytical model and a 2-layer isopycnic primitive equations numerical model have been used to examine an eddy's migration along a wall. The primary aim of this study was to discuss the three mechanisms determining the meridional migration of the eddy along the wall: the image effect, the β force, and the rocket effect, all of which appear to be of the same order of magnitude. We have extensively examined both quasigeostrophic and highly nonlinear eddies (lenses). The regime in between (i.e., moderately nonlinear eddies) received only a limited amount of attention. The results are summarized (for the Northern Hemisphere) as follows.

1) Among the three mechanisms, the image effect is always the most dominant in determining the eddy's final migration along the wall. Hence, a cyclonic eddy moves southward, and an anticyclonic eddy migrates northward.

2) The above is true even for highly nonlinear eddies such as anticyclonic lenses where our (misleading) intuition tells us that they should migrate southward (Fig. 4) rather than northward. This counterintuitive northward movement of lenses is made possible by the leakage of mass along the wall. The leakage plays a crucial role in the eddy–wall interaction process because it enables the center of the lens (i.e., the point of maximum pressure of the lens alone) to move northward (uphill), while the center of mass (of the lens and the leakage) may actually drift southward (downhill). Ultimately, the leakage destroys the ring by draining its entire fluid.

3) After an initially circular upper-oceanic eddy is driven toward a wall, its westward movement is arrested by a wall. For quasigeostrophic motions the eddy's shape and structure are drastically readjusted in such a way that a *wodon* is established [Eqs. (3.9)–(3.11) and Figs. 9, 11, and 12]. In other words, after the upper eddy's westward migration has been arrested by a wall [$t > (\beta R_d)^{-1}$], β no longer plays an important role in the eddy's migration. However, after a very long time [$t > (\mathrm{Ro}\beta R_d)^{-1}$] the eddy senses the changes in latitude and β becomes important again.

4) As the wodon solution involves a half-circular closed bounding streamline, leakage is not present. Hence, it can be qualitatively stated that the importance of the leakage increases with increasing nonlinearity. However, the specific manner by which the leakage role increases has not been established.

Possible application of this theory to rings generated by the East Australian Current and the Loop Current in the Gulf of Mexico is discussed. The impossibility of applying the theory at its present stage to warm core Gulf Stream rings is also examined.

Acknowledgments. The authors wish to acknowledge useful comments by M. E. Stern, W. Dewar, and S. Meacham. This study was supported by Office of Naval Research Grant N00014-89-J-1606 and by National Science Foundation Grants OCE-9012114 and OCE-9102025. It constitutes a part of Shi's Ph.D. dissertation.

REFERENCES

Bleck, R., and D. Boudra, 1986: Wind-driven spin-up in eddy-resolving ocean models formulated in isopycnic and isobaric coordinates. *J. Geophys. Res.*, **91,** 7611–7621.

Carnevale, G., R. Kloosterziel, and G. van Heijst, 1991: Propagation of barotropic vortices over topography in a rotating tank. *J. Fluid Mech.*, **233,** 119–139.

Chapman, D., and K. Brink, 1987: Shelf and slope circulation induced by fluctuating offshore forcing. *J. Geophys. Res.*, **92,** 11 741–11 759.

Cornillon, P., R. Weyer, and G. Flierl, 1989: Translation velocity of warm core rings relative to the slope water. *J. Phys. Oceanogr.*, **19,** 1317–1332.

Evans, R., K. Baker, O. Brown, and R. Smith, 1985: Chronology of warm-core ring 82B. *J. Geophys. Res.*, **90,** 8803–8811.

Flierl, G., 1984: Rossby wave radiation from a strongly nonlinear warm eddy. *J. Phys. Oceanogr.*, **14,** 47–58.

——, V. Larichev, J. McWilliams, and G. Reznik, 1980: The dynamics of baroclinic and barotropic solitary eddies. *Dyn. Atmos. Oceans,* **5,** 1–41.

Hamon, B., 1965: The east Australian current 1960–1964. *Deep-Sea Res.*, **12,** 899–921.

Kirwan, A., J. Lewis, A. Indest, P. Reinersman, and I. Quintero, 1988: Observed and simulated kinematic properties of loop current rings. *J. Geophys. Res.*, **93,** 1189–1198.

Lamb, H., 1932: *Hydrodynamics.* Dover, 738 pp.

Louis, J., and P. Smith, 1982: The development of the barotropic radiation field of an eddy over a slope. *J. Phys. Oceanogr.*, **12,** 56–73.

——, B. Petrie, and P. Smigh, 1982: Observations of topographic Rossby waves on the continental margin off Nova Scotia. *J. Phys. Oceanogr.*, **12,** 47–55.

Masuda, A., 1988: The skewed eddy of Batchelor-Modon type. *J. Oceanogr. Soc. Japan,* **44,** 189–199.

——, K. Marubayashi, and M. Ishibashi, 1987: Batchelor-modon type eddies and isolated eddies near the coast on an *f*-plane. *J. Oceanogr. Soc. Japan,* **43,** 383–394.

McWilliams, J., and G. Flierl, 1979: On the evolution of isolated, nonlinear vortices. *J. Phys. Oceanogr.*, **9,** 1155–1182.

Nakamoto, S., 1989: Soliton-like solutions in loop current eddies. *J. Geophys. Res.*, **94,** 14 567–14 574.

Nof, D., 1983: The translation of isolated eddies on a sloping bottom. *Deep-Sea Res.*, **30,** 171–182.

——, 1988a: Draining vortices. *Geophys. Astrophys. Fluid Dyn.*, **42,** 187–208.

——, 1988b: Eddy–wall interactions. *J. Mar. Res.*, **46,** 527–555.

Pedlosky, J., 1987: *Geophysical Fluid Dynamics.* Springer-Verlag, 710 pp.

Pierrehumbert, R., 1980: A family of steady, translating vortex pairs with distributed vorticity. *J. Fluid Mech.*, **99,** 129–144.

Saffman, P., 1979: The approach of a vortex pair to a plane surface in inviscid fluid. *J. Fluid Mech.*, **92,** 497–503.

Smith, D., 1986: A numerical study of Loop Current eddy interaction with topography in the western Gulf of Mexico. *J. Phys. Oceanogr.*, **16,** 1260–1272.

——, and W. Ulrich, 1990: An analytical theory of tropical cyclone motion using a barotropic model. *J. Atmos. Sci.*, **47,** 1973–1986.

Smith, D. C., IV, and J. J. O'Brien, 1983: The interaction of a two-layer isolated mesoscale eddy with bottom topography. *J. Phys. Oceanogr.*, **13,** 1681–1697.

Swaters, G. E., and G. Flierl, 1991: Dynamics of ventilated coherent cold eddies on a sloping bottom. *J. Fluid Mech.*, **223,** 565–587.

Umatani, S., and T. Yamagata, 1987: Evolution of an isolated eddy near a coast and its relevance to the "Kyucho." *J. Oceanogr. Soc. Japan,* **43,** 197–203.

Whitehead, J. A., M. E. Stern, G. R. Flierl, and B. A. Klinger, 1990: Experimental observations of baroclinic eddies on a sloping bottom. *J. Geophys. Res.*, **95,** 9585–9610.

Williams, G. P., and T. Yamagata, 1984: Geostrophic regimes, intermediate solitary vortices and Jovian eddies. *J. Atmos. Sci.*, **41,** 453–478.

Wu, H., E. Overman, and N. Zabusky, 1984: Steady-state solutions of the Euler equations in two dimensions rotating and translating V-states with limiting cases. I: Numerical algorithms and results. *J. Comput. Phys.*, **53,** 42–71.

Yasuda, I., K. Okuda, and K. Mizuno, 1986: Numerical study on the vortices near boundaries—considerations of warm core rings in the vicinity of the east coast of Japan. *Bull. Tohoku Reg. Fish. Res. Lab.*, **48,** 67–86.

Zalesak, S., 1979: Fully multidimensional flux-corrected transport algorithms for fluids. *J. Comput. Phys.*, **31,** 335–362.